Re-entrant Nematic Behavior in the 7OCB+9OCB Mixtures: Evidence for Multiple Nematic−Smectic Tricritical Points

Paul Cusmin,[†] Josep Salud,[†] David O. López,*[,†] Maria R. de la Fuente,[‡] Sergio Diez,[†] Miguel A. Pérez-Jubindo,[‡] María Barrio,[†] and Josep Ll.Tamarit[†]

Laboratori de Caracterització de Materials (LCM), Departament de Física i Enginyeria Nuclear, E.T.S.E.I.B. Universitat Politècnica de Catalunya, Diagonal, 647 08028 Barcelona, Spain, and Departamento de Física Aplicada II, Facultad de Ciencias, Universidad del País Vasco, Apartado 644, E-48080 Bilbao, Spain

Received: July 5, 2006; In Final Form: October 4, 2006

The metastable phase diagram of the two-component system heptyloxycyanobiphenyl (7OCB)+nonyloxycyanobiphenyl (9OCB) was determined by means of modulated differential scanning calorimetry (MDSC) and optical microscopy measurements. It was experimentally established that the 7OCB+9OCB two-component system exhibits a monotropic re-entrant nematic behavior. A complete quantitative thermodynamic analysis, through Oonk's equal *G* analysis, was performed, allowing for the calculation of the monotropic re-entrant behavior and the prediction of two tricritical points, one of them experimentally accessible for the SmA_d-to-N transition and the other non-experimentally accessible for the RN-to-SmA_d transition. From specific-heat measurements, latent heats were obtained for those mixtures displaying a first-order SmA_d-to-N transition. Additionally, for some mixtures, the specific-heat critical exponents (α), through the second-order SmA_d-to-N transition, were obtained. Both batches of data enable us to access to the experimental tricritical temperature for the SmA_d-to-N transition.

1. Introduction

There exist certain kinds of liquid crystal materials that display some common features. One such feature is that the constituent molecules have strongly polar end groups and a smectic A phase in which the layer spacing d varies, $l < d < 2l$ (where l denotes the length of the molecule) (named partial bilayer smectic A (SmA_d)). In addition, under certain conditions (either by pressure or by making appropriate mixtures with other selected materials), these materials exhibit a nonstandard mesophase sequence upon cooling the sample from the isotropic phase (I): (N) nematic, (SmA_d) bilayer smectic A, and nematic again, denoted as re-entrant nematic (RN).

Although the re-entrant behavior was first discovered by P.E. Cladis in the 1970s for mixtures of two polar paracyano-substituted liquid crystals at atmospheric pressure,[1] this phenomenon can be found in other materials such as pure iron, superconducting materials, vapor−liquid systems, and even in nonpolar liquid crystals.[2,3] The common fact, irrespective of the chosen material, is that less ordered phases exist at higher temperatures. It seems that in all these cases the return to a disordered state with decreasing temperature is caused by competing order parameters. In liquid crystals, both the smectic and nematic order parameters can be successfully evaluated from experimental procedures as well as by applying, among others, theoretical formulations based on mean-field approaches. Thus, the re-entrant nematic phenomenon in liquid crystals has resulted in extensive theoretical and experimental studies.

The first theoretical attempts to understand the re-entrance in nematic liquid crystals were performed by P.E. Cladis et al.[4,5] who proposed a microscopic model of a bilayer smectic A and a qualitative explanation of how the SmA_d-to-N phase transition might occur. Soon after, a phenomenological Landau description was proposed[6,7] and even a refined Landau description based on microscopic considerations.[8] Microscopic theories came up everywhere, although, among them, maybe at first, the most successful one in reproducing quantitatively the observed re-entrant behavior was the frustrated spin-gas model.[9−11] In the 1990s and up to the present time, this model was substantially developed[12] and other microscopic-related approaches have also been proposed.[13−15] In parallel to the microscopic theories, pure thermodynamic procedures were used as early as the 1970s to calculate the phase boundaries in the pressure−temperature or composition−temperature planes. The pioneers Klug and Whalley[16] and independently Clark[17] fitted the experimental results (temperature−pressure or temperature−composition) to either an ellipse or a parabola using a quadratic expansion in temperature and pressure or composition for the difference of Gibbs energy functions between the smectic and nematic phases. A general and simple thermodynamic approach to get phase boundaries in composition−temperature planes was proposed shortly after (denoted as Oonk's thermodynamic equal Gibbs-analysis).[18] Soon after, Van Hecke,[19] through Oonk's method, and later Sorenson and Van Hecke,[20] successfully reproduced and quantified the re-entrant nematic behavior in a two-component system (composition−temperature plane). The Van Hecke extension of Oonk's method could only be applied to first-order transitions for which the entropy changes are not zero. According to this fact, about 3 years ago, some of the authors of the present paper reproduced, by means of Oonk's method following the Van Hecke's procedure (assuming an extremely small absolute entropy change but different from zero), the

* Author to whom correspondence should be addressed. E-mail: david.orencio.lopez@upc.es.
[†] Laboratori de Caracterització de Materials (LCM).
[‡] Departamento de Física Aplicada II.

10.1021/jp0642286 CCC: $33.50
Published on Web 12/08/2006

second-order re-entrant nematic behavior in the heptyloxycyanobiphenyl (7OCB)+octyloxycyanobiphenyl (8OCB) binary mixtures.[21]

A huge amount of measurements of different properties with different techniques has been performed since the 1970s. If only classic liquid crystals of the series of alkylcyanobiphenyls (*n*CB, where *n* denotes the number of carbons in the alkyl chain) and alkyloxycyanobiphenyls (*n*OCB, where *n* has the same meaning as the former) are taken into account (some of them are known to exhibit SmA_d), the re-entrant nematic phenomenon was studied by means of specific-heat measurements,[22,23] X-ray diffraction techniques,[7,24−26] optical experiments,[22,24,27−30] NMR dynamic determinations,[31−34] dielectric spectroscopy,[35−37] viscosity measurements,[38,39] and high-resolution volumetric determinations.[7,40,41] In particular, the 6OCB+8OCB mixtures have been broadly[7,16,20,22,24−27,31−36,39,41] studied, probably because they are some of the first two-component systems where re-entrance was observed and, above all, because a stable re-entrant nematic phase is present in an adequate temperature range. One might expect that re-entrance occurs for mixtures of compounds belonging to the same series or even to homologous series, chosen in such a way that a member without a smectic phase is mixed with a member displaying a SmA_d phase. Following this line of reasoning and focusing on the *n*OCB series of compounds, the longest *n*OCB compound that does not display SmA_d is 7OCB, and so, the 7OCB+8OCB two-component system displays re-entrant nematic behavior, as it has been recently proved.[21] However, unlike the 6OCB+8OCB two-component system, the re-entrant nematic behaviors of the 7OCB+8OCB mixtures are only attained on cooling being monotropic or metastable. Other possibilities of re-entrance, on the same *n*OCB series, could emerge from the 7OCB+9OCB mixtures.

In the work dealt with in this paper, we have carried out modulated differential scanning calorimetry (MDSC) and optical measurements in order to completely characterize the 7OCB+9OCB two-component system. The interest in these mixtures arises from both the theoretical and experimental aspects. It seems that the pure 9OCB compound displays a SmA_d-to-N phase transition of first-order in nature.[42] When mixing with the nematic 7OCB liquid crystal, the experimental results confirm the existence of a monotropic re-entrant nematic phase in such a way that the nematic range NR ($=T_{NI}-T_{AN}$, where T_{NI} is the nematic to isotropic transition temperature and T_{AN} is the smectic to nematic transition temperature) increases for 7OCB-richer mixtures. That is to say, the ratio T_{AN}/T_{NI}, also called McMillan's ratio,[43] decreases. According to the MKG theory developed by McMillan,[43] Kobayashi,[44] and de Gennes,[45] the SmA-to-N transition should belong to the 3D-XY-Universality class. However, owing to a coupling between nematic and smectic order parameters, strongly influenced by the extension in temperature of the nematic range, a crossover behavior from the strict second-order transition up to the tricritical point (TCP, beyond which the SmA-to-N transition becomes first-order in nature) is observed. The stronger the coupling occurs the more McMillan's ratio approaches 1. In contrast, the 3D-XY model is only applicable when the nematic order is completely saturated. This takes place when the coupling is weak enough or, in terms of McMillan's ratio, when T_{AN}/T_{NI} is small enough. In our case, a TCP in the SmA_d-to-N phase transition is expected to exist for 7OCB+9OCB mixtures in addition to the re-entrant behavior. At this point, it is very interesting to elucidate how the TCP temperature and the re-entrant temperature (the limit temperature below which the RN mesophase appears) are located in the smectic−nematic phase boundary in the composition−temperature plane. A complete thermodynamic analysis has been addressed to reproduce the re-entrant nematic behavior through Oonk's equal-Gibbs analysis following Van Hecke's procedure. In addition, the procedure has been modified for second-order phase transitions, imposing strictly zero entropy change, in order to predict the TCP temperature. What perhaps is not yet evident to the best of our knowledge, it is the occurrence of more than one TCP that has been unexpectedly inferred from this thermodynamic analysis. Finally, such calculations have been extended to the crystalline solid state to obtain information about the complete two-component system 7OCB+9OCB.

The paper is organized as follows. In Section 2, we describe the experimental details. In Section 3, the results addressed to the experimental determination of the monotropic re-entrant phase diagram are displayed. First- and second-order SmA_d-to-N phase transitions are analyzed in Sections 4 and 5, respectively. In Section 6, the basis of Oonk's equal-Gibbs method along with re-entrant behavior calculations are exposed. The discussion is driven in two ways: first, a tentative stable melting phase diagram is proposed with the aid of the thermodynamic equal-Gibbs analysis, and second, the occurrence of multiple tricritical points through the smectic−nematic transition is discussed. Finally, in Section 8, a summary of the main conclusions is made.

2. Experimental

2.1. Materials. The pure components 7OCB and 9OCB were synthesized and purified by Dabrowsky in the Institute of Chemistry, Military University of Technology, Warsaw, Poland. The purity was stated to be higher than 99.9%, and no further purification was made. Both liquid crystals display well-known phase sequences upon heating: Cr (crystal) 327.22 K (89.23 J K^{-1} mol^{-1}) N (nematic) 347.31 K (0.891 J K^{-1} mol^{-1}) I (isotropic) for 7OCB[21,46,47] and Cr (crystal) 336.95 (105.179 J K^{-1} mol^{-1}) K SmA (smectic A) 351.08 K (0.456 J K^{-1} mol^{-1}) N (nematic) 353.22 K (2.378 J K^{-1} mol^{-1}) I (isotropic) for 9OCB.[21]

Liquid crystal binary mixtures of 7OCB+9OCB were prepared at room temperature by weighing the pure components in selected proportions. To obtain homogeneous mixtures, samples were sealed in aluminum pans, heated up to isotropic phase, and annealed for a period of several weeks.

2.2. MDSC Technique. The MDSC technique enables to perform measurements as in a conventional DSC calorimeter, as well as in modulated mode. In such a mode, the conventional temperature program (usually a linear-time temperature program) is superimposed with a periodic temperature change (usually sinusoidal) that constitutes the perturbation. The response is embodied in the heat flow rate that, by means of an appropriate mathematical procedure, can deconvolute the response to the perturbation (a dynamic component arising from the temperature modulation) from the response to the conventional linear-time temperature program (an underlying heat flow rate, which is approximately the conventional DSC heat flow). This technique provides the ability to measure, under suitable conditions (linear response and steady state), the specific heat directly in a single experiment and to measure it even at very slow underlying heating rates. Its design makes it also suitable for quantitative measurements of latent heats of first-order transitions, even if they are weak. In addition, by measurement of phase shift changes, MDSC provides an intrinsic method to determine the character of a phase transition. More details on the MDSC technique can be found in the literature.[42,48,49]

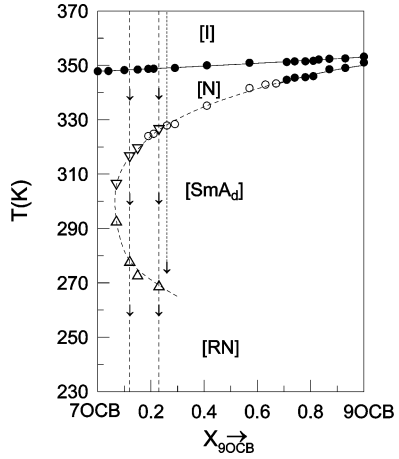

Figure 1. Partial phase diagram for 7OCB+9OCB mixtures showing monotropic re-entrant nematic behavior. The open and filled circles correspond to specific-heat measurements by means of MDSC technique. Up-and-down triangles correspond to optical measurements. Down arrows in vertical dashed lines correspond to a set of microscopic measurements. Vertical dotted line corresponds to a representative mixture for which specific-heat and optical measurements have been recorded.

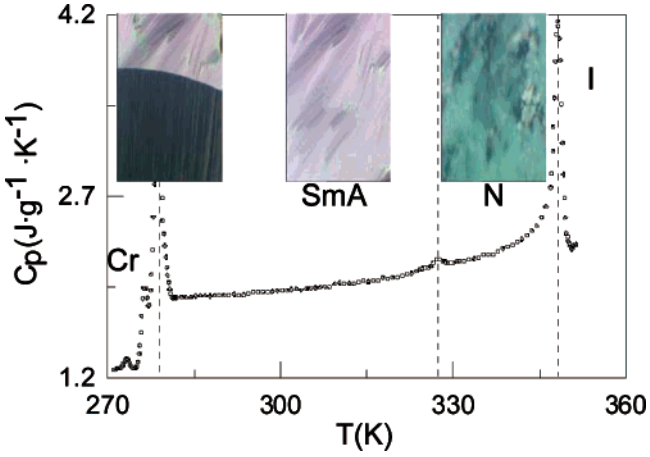

Figure 2. Specific-heat data along with some photographs showing the textures of the different phases for the representative mixture $X_{9OCB} = 0.26$. All the data were obtained on cooling from the isotropic phase at a scanning rate of 1 K min^{-1}.

Two sorts of MDSC measurements were made. In one type, cooling was performed from the isotropic phase (or heating from the SmA$_d$-phase) with a scanning rate of 1 K min^{-1}, a modulated temperature amplitude of $\pm$ 0.5 K, and a modulation period of 60 s. The second batch of measurements consisted of heating from the SmA phase at 0.01 K min^{-1} with a modulation temperature amplitude of $\pm$ 0.035 K and a period of 25 s. In both cases, the chosen parameters enabled us to obtain a linear response and a steady state. The sample masses were selected to ensure a uniform thin layer within the aluminum pan. The specific-heat calibration was carefully performed using pure synthetic sapphire, as the accuracy in the absolute value was not better than 5%.

In order to obtain the complete two-component system, standard DSC measurements were made on various selected mixtures and pure components. The scanning rates were 2 K min^{-1}, and the sample masses were chosen between 5 and 10 mg.

2.3. Optical Microscopy. The microscopy observations were made with an Olympus polarizing microscope equipped with a Linkam THMSG-600 hot stage and a Linkam TMS-94 temperature controller. The sample cells (one from Linkam, thickness 5 μm and another from EHC, thickness 25 μm) were filled by capillarity with the liquid crystal in its isotropic phase. The cooling and heating rates were 2 K min^{-1}.

3. Re-entrant Nematic Phase Behavior

In Figure 1, the partial phase diagram of 7OCB+9OCB, showing a monotropic re-entrant nematic (RN) behavior, is depicted. This figure includes transition temperatures for the RN-to-SmA$_d$, SmA$_d$-to-N, and N-to-I phase transitions obtained from MDSC calorimetry working in modulated mode (specific-heat data) as well as from optical microscopy. The full circles (all of them obtained from MDSC calorimetry) represent temperatures corresponding to first-order transitions (as indicated by δ-phase shift measurements), i.e., the N-to-I phase transition for pure components and their mixtures and a part of the SmA$_d$-to-N phase transition, beyond the TCP composition at the 9OCB-rich side of the two-component system. Although a two-phase equilibrium is experimentally found, it is very narrow (the MDSC technique allows us to observe a minimum coexistence region $\sim$0.05 K wide), and for simplicity, a single continuous line has been drawn. In contrast, when the transition is second-order in nature (open symbols), there is no phase coexistence region and only one line is required. This takes place at the SmA$_d$-to-N phase transition for mixtures with larger content in 7OCB than the TCP composition and possibly at the RN-to-SmA$_d$ phase transitions for which, in all these cases, a dashed line has been plotted. It is important to realize that open circles come from MDSC experiments whereas up-and-down empty triangles come from optical microscopy working on cooling mode from the isotropic phase.

In Figure 2, the trend of the specific heat along with optical textures (the sample in inhomogeneous alignment) of different phases for a representative mixture (X_{9OCB}=0.26) in a cooling run experiment (at 1 K min^{-1}) is shown. As can be observed, a very small specific-heat peak for the N-to-SmA$_d$ transition is detected. In addition, at lower temperatures, only a twined specific-heat peak is observed. Optical texture doubtless points out that this specific-heat peak corresponds to the transition at which the supercooled SmA$_d$-mesophase crystallizes. All attempts to detect the SmA$_d$-to-RN specific-heat peak either for this composition or in other mixtures with larger content of 7OCB were unsuccessful, even by modifying the cooling rate.

The RN phase has only been detected by means of optical measurements on cooling run experiments from the isotropic phase, fast enough (at 2 K min^{-1}) to prevent the supercooled SmA$_d$-mesophase from crystallizing. In Figure 3, the optical textures for the two different compositions (X_{9OCB}=0.12 and 0.23) as examples are shown at several temperatures. Those textures corresponding to $X_{9OCB} = 0.23$ were obtained with EHC cells in an inhomogeneous alignment. As can be observed, only two different textures are clearly shown down to 351 K, the temperature at which an almost perfect black texture representative of an I phase is obtained. The first one, at temperatures such as 340 K, shows a typical green nematic−Shlieren texture. At lower temperatures, such as 300 K, the Shlieren texture changes to a fan-shaped focal conic texture characteristic of a SmA$_d$ mesophase. If the sample is still cooled down (e.g., to 260 K), a green Shlieren texture is reverted and then assigned to a nematic-like mesophase, denoted RN. As can be observed in the photo at the right-bottom side, at lower temperatures, the metastable RN mesophase crystallizes, forming circular domains.

The textures corresponding to $X_{9OCB} = 0.12$ in Figure 3 were obtained by means of Linkam cells in perfect parallel alignment.

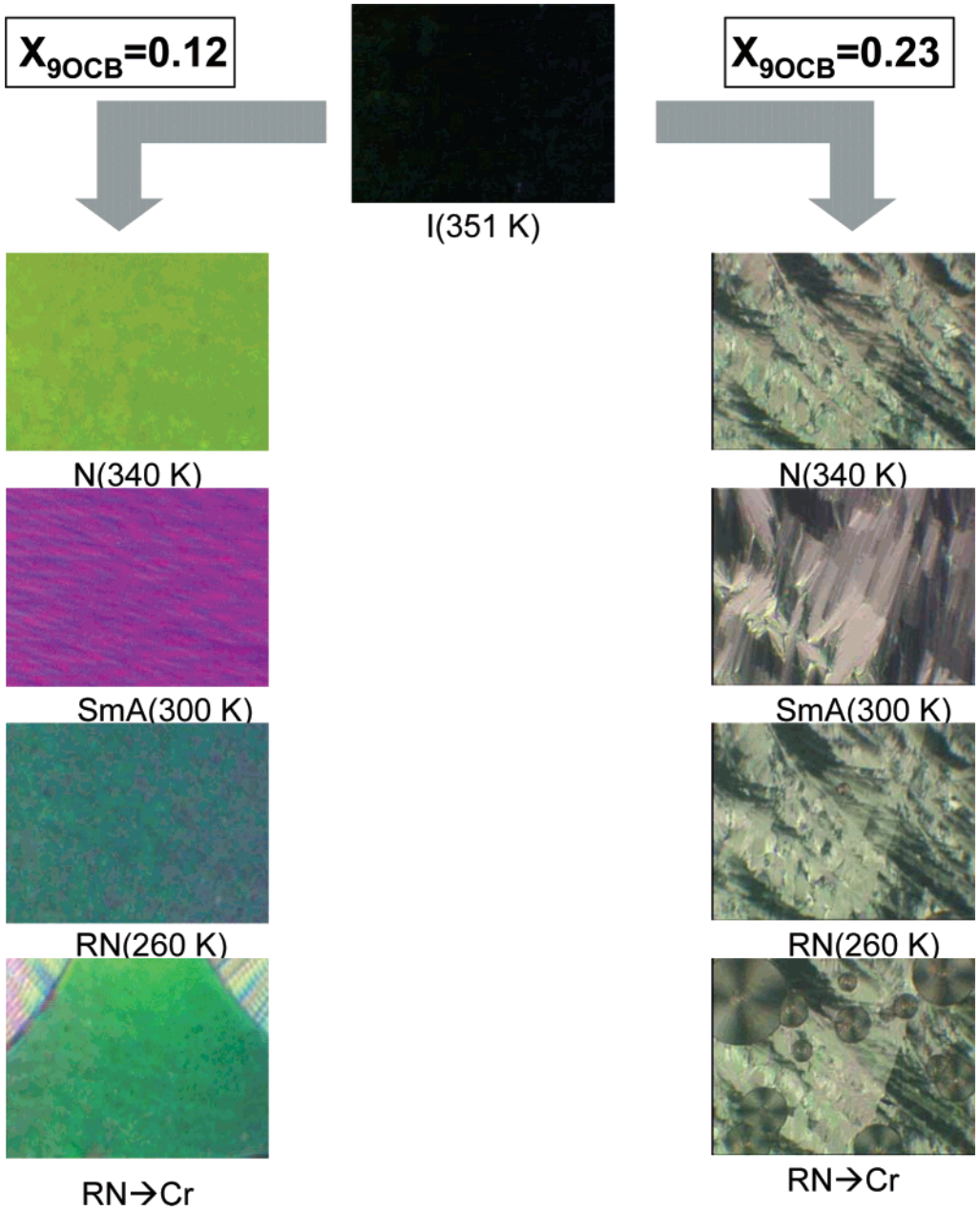

Figure 3. Sequence of photographs showing the textures for mixtures $X_{9OCB} = 0.12$ (planar alignment) and 0.23 (inhomogeneous alignment) at several temperatures.

In such a case, green photos correspond to nematic-like mesophases obtained at 340 and 260 K, whereas the photo at an intermediate temperature (300 K), in which a purple texture is observed along with diagonal lines representing the smectic planes, is characteristic of a SmA_d mesophase. The photo at the left-bottom side shows how the RN mesophase (green texture) crystallizes to form circular domains. All temperatures in Figure 3 were marked in Figure 1 by means of black down arrows on the representative dashed lines.

4. First-Order SmA_d-to-N Phase Transition

The extension of the first-order character of the SmA_d-to-N phase transition in the mixtures has been investigated through δ-phase shift data as well as by the determination of latent heats. The occurrence of a weak first-order phase transition can be detected by a peak in the evolution of the δ-phase shift with temperature located at the same temperature as the specific-heat peak. This peak is believed to be associated with the existence of latent heat in such a way that the less the δ-peak is observed the less the latent heat should be found. At the insets of Figure 4, in the same δ-scale, some representative mixtures have been chosen to show, in the vicinity of the SmA_d-to-N phase transition, the δ-values against $(T - T_{peak})$ in which T_{peak} is defined as the specific-heat temperature peak. As can be seen, a δ-peak is clearly observed for the mixture $X_{9OCB} = 0.93$, attenuating for mixtures with larger content in 7OCB. In particular, for the mixture $X_{9OCB} = 0.67$, no δ-peak seems to exist. This means that the order of the SmA_d-to-N transition must change for a composition such as 0.67 in mole fraction of 9OCB or close to it. To get a more accurate experimental location of the TCP composition, the latent heat ΔH_{SmA-N} has been obtained. It should be noted that the latent heat associated with a first-order discontinuity in the enthalpy change has been proven to be difficult to obtain with the required accuracy. For

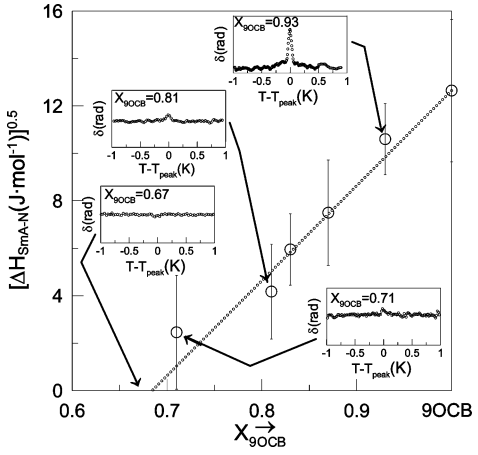

Figure 4. Square-root latent heat ($[\Delta H_{SmA-N}]^{0.5}$) against composition for several mixtures of 7OCB+9OCB. The insets show, in the same-scale, the δ-phase shift data against ($T - T_{peak}$) through the SmA_d-to-N phase transition for several representative 7OCB+9OCB mixtures.

a given experiment, it is important to define the total enthalpy change:

$$\Delta H^{TOT}_{SmA-N} = \Delta H_{SmA-N} + \int \Delta C_p \, dT \qquad (1)$$

where the last term of the right-hand of eq 1 is the pretransitional fluctuation contribution ($\Delta C_p \equiv C_p - C_{p,background}$ is the excess specific heat due to the change in ordering associated with the transition). If a phase transition is of second-order, the latent heat ΔH_{SmA-N} vanishes. The MDSC technique enables us to determine, in a direct manner, both right terms in eq 1. As early as 1984, Thoen and co-workers,[50] and more recently some of us,[42,51,52] pointed out that a linear relationship can be obtained when $(\Delta H_{SmA-N})^{0.5}$ vs composition is plotted. Likewise, it was revealed as an excellent experimental procedure to get the tricritical composition with a certain accuracy. In Figure 4, the $(\Delta H_{SmA-N})^{0.5}$ data for certain 7OCB+9OCB mixtures against composition are presented. As can be easily observed, the linear fit extrapolation leads to a zero value for $X_{9OCB} \approx 0.69$ (the error quoted from the fitting procedure is estimated to be about 0.05 in mole fraction). The latent heat for the mixture $X_{9OCB} = 0.67$ is experimentally estimated to be zero or extremely low in relation to the experimental uncertainty.

5. Second-Order SmA_d-to-N Phase Transition

The study of the second-order SmA_d-to-N transition was performed by measuring the specific-heat data of some binary mixtures at 0.01 K min^{-1} ($\Delta T = \pm 0.035$ K, $T = 25$ s, the proposed conditions described in Section 2). These C_p data were analyzed through the renormalization-group expression[53]

$$C_p^{\pm} = B + E\epsilon + A^{\pm}|\epsilon|^{-\alpha}[1 + D^{\pm}|\epsilon|^{0.5}] \qquad (2)$$

where $\pm$ indicates above and below the transition. The temperature at which the smectic and nematic behaviors diverge is the critical temperature T_c. The reduced temperature is ϵ (= $(T - T_c)/T_c$). The corresponding amplitudes above and below are $A^{\pm}$, whereas the constants B and E account for the specific-heat background, both being above and below the transition. The specific-heat critical exponent is α, also the same above and below the transition. The first-order correction to scaling term is $D^{\pm}|\epsilon|^{0.5}$, which was added to the simple power law expression to guarantee the smooth variation of the background at T_c. We fixed the exponent of this term at the value 0.5 (essentially the 3D-XY value of 0.524 predicted for the model), and no additional fit was tried. The theory for the 3D-XY universality class predicts an amplitude ratio (A^-/A^+) of 0.971, a critical exponent α of -0.007, and a D^-/D^+ ratio of 1. These predictions are different around the TCP; here, A^-/A^+ is about 1.6, the critical exponent α is 0.5, and D^-/D is close to 1. Equation 2 is often used for pure liquid crystal compounds, although it can also be used for mixtures of homologous compounds.[42,52] Given that, for the mixtures dealt with in this work, the measurements are performed at a constant mole fraction and no indications of Fisher renormalization are observed,[42,51,52] it seems physically reasonable that no significant distinction exists with regard to the measurements performed at constant chemical potential difference.

The results of fits using eq 2 (α, A^-/A^+, D^-/D^+, T_c) over the range $|\epsilon| \leq 5 \times 10^{-3}$ are presented in Table 1 for some analyzed mixtures of the two-component system 7OCB+9OCB for which a second-order SmA_d-to-N transition is assumed to exist. All the parameter sets represent well enough the measured specific-heat data, as indicated by χ^2 values. It should be noticed that there was a certain difficulty in fitting the α-critical exponent with the constraint $\alpha^+ = \alpha^-$ for the mixture $X_{9OCB} = 0.57$, as is reflected by the abnormal D^-/D^+ fitted ratio (see Table 1), although the set of fitted parameters reproduces, via eq 2, quite well the measured specific heat around the SmA_d-to-N transition, as can be seen in Figure 5. In fact, the more 7OCB content, the smaller the C_p peak is. This fact, also observed by us for 7OCB+8OCB mixtures,[21] was explained by Kortan et al.[26] from X-ray measurements performed on 6OCB+8OCB mixtures as being due to an increasing of the correlation volume for those mixtures as the re-entrance comes closer. For 7OCB+9OCB mixtures, no C_p peak is observed for $X_{9OCB} < 0.2$. At $X_{9OCB} = 0.41$, the C_p peak is about 4 times smaller than that found at $X_{9OCB} = 0.67$ (Figure 5). No fittings following eq 2 have been consigned in Table 1 for mixtures with mole fractions lower than $X_{9OCB} = 0.57$ due to the poorly fitted parameters.

6. Thermodynamic Analysis

6.1. Oonk's Equal-Gibbs Energy Analysis. Under isobaric conditions, the thermodynamic properties of a binary mixture of a two-component system A+B can be determined if, for each possible phase of this mixture, the molar Gibbs energy as a function of temperature and composition is known. The Gibbs energy function of a phase α is described by the following expression in terms of X moles of B and $(1 - X)$ moles of A (i.e., the mixture $A_{1-X}B_X$)

$$G^{\alpha}(X,T) = (1 - X)\mu_A^{*,\alpha}(T) + X\mu_B^{*,\alpha}(T) + RT[(1 - X)\ln(1 - X) + X\ln X] + G^{E,\alpha}(X,T) \qquad (3)$$

where $G^{E,\alpha}(X,T)$ is the excess Gibbs energy, $\mu_A^{*,\alpha}$ and $\mu_B^{*,\alpha}$ are the molar Gibbs energies of the pure components, R is the gas constant, and T is the thermodynamic temperature.

To determine an arbitrary first-order two-phase equilibrium region between two phases α and β at each temperature in a two-component phase diagram, the traditional criterion of equilibrium is satisfied by the double tangent line to the minimum Gibbs energy functions giving rise to the equilibrium compositions (X_α and X_β). However, when the transition entropies of the pure compounds are very small, both compositions are very close and it results in a very narrow two-phase region. In addition, these compositions are very close to the intersection of both Gibbs energy functions, named equal Gibbs composition (EGC).

TABLE 1: Results of Fits to Eq 2 for Some Mixtures of the 7OCB+9OCB Two-Component System for which a Second-Order SmA_d-to-N Phase Transition Exists[a]

X_{9OCB}	N	α	A^-/A^+	D^-/D^+	T_c (K)	$\chi^2 \times 10^3$
0.67	350	0.43 ± 0.04	1.1 ± 0.4	1.0 ± 0.1	342.81 ± 0.41	1
0.63	342	0.38 ± 0.03	0.6 ± 1.5	1.5 ± 1.9	342.43 ± 0.60	2
0.57	350	0.26 ± 0.08	1.2 ± 1.5	15.4 ± 15[b]	341.11 ± 0.35	5

[a] N is the number of data points included in these fits. The errors quoted are the statistical uncertainties. [b] This value reflects a great difference between D^- and D^+ forced by the fitting procedure to get the same value of α below and above the transition.

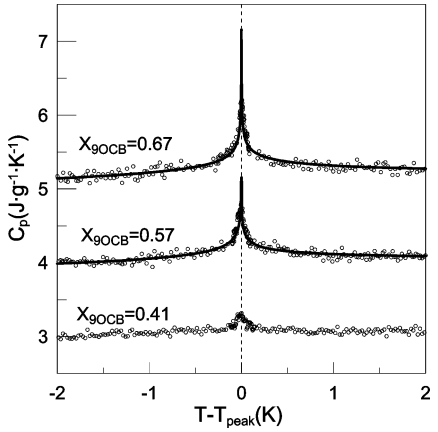

Figure 5. Experimental specific-heat data (○) for the mixtures $X_{9OCB} = 0.67$, 0.57, and 0.41 against $(T - T_{peak})$ through the SmA_d-to-N phase transition. Continuous lines are fittings according to eq 2. The data have been shifted from that corresponding to $X_{9OCB} = 0.41$ in order to facilitate comparison.

This EGC changes with temperature, giving rise to the EGC curve (EGCC),[18] which in a practical sense provides the representative line of the very narrow two-phase equilibrium in a T−X plot. In the limit, in which the phase transition is purely second-order in nature, the transition entropies of the pure compounds are considered to be zero, both equilibrium compositions and the EGC are equal, and no coexistence region exists because both Gibbs energy functions coincide at every temperature and composition. What is really interesting is what happens when for a pure component the entropy change is considered to be zero whereas for the other is small but different from zero. In such a case, both Gibbs energy functions would coincide at a given temperature, only for a certain composition range. To the best of our knowledge, this particularity has been used in the work dealt with in this paper, for a first time, to predict by means of thermodynamic considerations the tricritical temperature in the smectic−nematic phase transition at which a weakly first-order two-phase equilibrium region changes to a second-order line.

Setting eq 3 for the α-phase equal to its parallel for the β-phase will give the EGC curve equation

$$G^{\alpha}(X,T) - G^{\beta}(X,T) = (1 - X)\Delta\mu^*_A(T) + X\Delta\mu^*_B(T) + \Delta G^E(X,T) = 0 \quad (4)$$

where $\Delta\mu^*_i(T) = \mu^{*,\alpha}_i - \mu^{*,\beta}_i$ (i = A,B). To proceed further, expressions are required for $\Delta\mu^*_i(T)$ and $\Delta G^E(X,T)$. For $\Delta\mu^*_i(T)$, using the transition temperature as a reference point, we have

$$\Delta\mu^*_i = -\Delta S^*_i(T - T_i) + \Delta C^*_{pi}(T - T_i - T\ln(T/T_i)) \quad (5)$$

where ΔS^*_i is the transition molar entropy change and ΔC^*_{pi} is the one in specific heat, both at the transition temperature T_i. It should be noted that ΔC^*_{pi} is taken to be the first-order difference in the specific heats between α and β phases. It should also be noted that if the transition α to β were purely second-order, ΔS^*_i would be 0 and $\Delta\mu^*_i$ is entirely determined by the change in specific heat.

For $\Delta G^E(X,T)$, a two-parameter form of the Redlich−Kister expansion is commonly used

$$\Delta G^E(X,T) = X(1 - X)[\Delta A_1(T) + \Delta A_2(T)(1 - 2X)] \quad (6)$$

where $\Delta A_i(T)$ values are usually taken to be constant or a function of temperature in the form $\Delta H^E_i - T\Delta S^E_i$.

The EGC method requires some experimental data related to the phase transition of the mixtures in order to perform an iterative procedure in which one obtains a reasonable EGC curve as well as the $\Delta G^E(X,T)$ along this curve. This procedure can be automatically executed by means of the WINIFIT 2.2-software[54] (based upon the old version WINIFIT 2.0, which has been slightly modified to include the possibility of strictly zero entropy change for pure components).

Re-entrant phase behavior in an arbitrary two-component system A+B can be attained by means of the EGC method following Van Hecke's procedure.[19] In such a procedure, one of the pure components, for example compound B, must exhibit re-entrant behavior (α-to-β at T^L_B and β-to-α at T^H_B), and in addition, both phase transitions must be first-order. For compound A, which does not exhibit re-entrant behavior, the α-to-β phase transition is absent, although it could exist as virtual (between α and metastable β) at temperatures low enough ($T \leq T^L_B$). More details on the procedure can be found elsewhere.[19,21]

6.2. Thermodynamic Calculation of the Re-entrant Nematic Phase Behavior. A thermodynamic G analysis of the monotropic re-entrant phase diagram depicted in Figure 1 must be performed by analyzing as a first step the first-order N-to-I phase transition in pure components and their mixtures ([N+I] two-phase equilibrium), followed by the SmA_d-to-N transition that exhibits a monotropic re-entrant nematic behavior.

According to eq 3, one Gibbs energy function is needed for the I phase and another for the N phase. The required input for the theoretical analysis includes the experimental data points read from Figure 1 together with the experimental thermal properties of the pure components corresponding to the first-order N-to-I transition read from Section 2.1. The EGC method, via WINIFIT, provides the excess Gibbs energy difference between N and I phases along the EGCC (given by an expression similar to eq 6) with the coefficients taken as temperature-independent

$$\Delta G^E(X) = G^{E,I} - G^{E,N} = X(1 - X)[-8.8\ (\pm 0.5) + 0.2\ (\pm 1.0)(1 - 2X)]\ \text{J mol}^{-1} \quad (7)$$

Phase I will be assumed to be strictly ideal in further calculations, and absolute values of the coefficients in eq 7 will

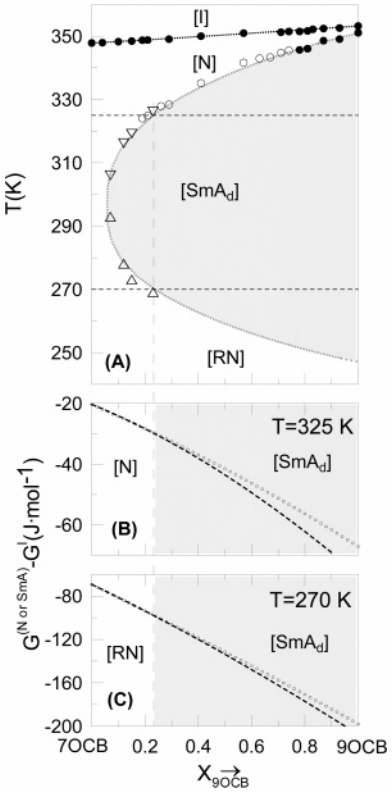

Figure 6. (A) Calculated partial phase diagram for 7OCB+9OCB mixtures showing monotropic re-entrant nematic behavior. The symbols have the same meaning as consigned in Figure 1. Calculated both ($G^N - G^I$) (○○○○) and ($G^{SmA} - G^I$) (dashed lines) (B) at 325 K and (C) at 270 K, plotted against composition.

be considered for the N phase. As this equilibrium is very narrow, only the EGCC has been drawn for simplicity in Figure 6A.

The SmA_d-to-N transition can also be calculated using WINIFIT by comparing the Gibbs energy curves of the N and SmA_d phases. To do so, a virtual second-order SmA_d-to-N phase transition for 7OCB has to be considered for eq 4 to be applied. For that phase transition, the entropy change is considered to be zero and both transition temperature and specific-heat change must be estimated by means of WINIFIT software from the experimental data points of the mixtures consigned in Figure 1. The virtual transition temperature (metastable SmA_d-to-N) is estimated to be 235 K, a value different from that estimated for us in a previous work[21] for the same virtual transition in 7OCB, but it satisfies the condition that no transitions from the SmA_d-to-N phase are allowed for 7OCB in the temperature range between T_B^H and T_B^L. Possibly, such a discrepancy could be due to the procedure of the calculation. In the present calculation (unlike previous calculations), a strictly zero entropy change has been imposed. As for the specific-heat change attributed to the virtual SmA_d-to-N transition, we used the previously published value[21] 0.002 J mol^{-1} K^{-1}. As for 9OCB, both the entropy change and transition temperature are experimentally known. The specific-heat term of eq 5 responsible for the re-entrance in 9OCB has to be estimated. In principle, it can be used as a parameter to be adjusted by means of WINIFIT, the best value being 2.67 J mol^{-1} K^{-1}. Its physical coherence was experimentally tested from highly accurate specific-heat data for pure 9OCB[55] as well.

Finally, the excess Gibbs energy obtained for the SmA phase is

$$G^{E,SmA}(X) = X(1-X)[19.2\ (\pm 0.2) + 1.2\ (\pm 0.4)(1-2X)]\ \text{J mol}^{-1} \quad (8)$$

The calculated EGCC, drawn in Figure 6A, reproduces quite well the experimental re-entrant nematic behavior. The T_{9OCB}^L temperature, not experimentally accessible because of its supercooled metastable character, could be estimated to be 247 K. The re-entrant nematic temperature is found to be about 298 K.

The Gibbs energies G^N and G^{SmA} for which the G^I phase has been subtracted, calculated using WINIFIT, at 325 and 270 K are shown in Figures 6B and C, respectively. This representation provides the same mesophase (SmA_d or N) stability to what is found when G^N and G^{SmA} are directly plotted, although in this case both G curves are almost identical and no stability can be inferred at a first glance. Figures 6B,C enable us to better distinguish the small differences and then to observe the mesophase stability. It should be noticed that the EGC composition also comes from the intersection of both sets of Gibbs energy differences ($G^{SmA} - G^I$) and ($G^N - G^I$). It is also very important to observe from Figures 6B,C that this EGC seems to be extended over a composition range (left side in both figures) as due to the second-order character. In this composition range both, G^N and G^{SmA} are identical in such a way that no differences in Gibbs energy seem to exist. On the right side, the stability of the SmA_d mesophase can be clearly observed.

7. Discusssion

7.1. Stable Melting Phase Diagram. Pure compound 7OCB displays a rather complicated solid-crystalline polymorphism, as has been recently discussed.[21] It seems from thermal experimental data that 9OCB likely presents a comparable solid-crystalline polymorphism in which several crystalline metastable phases can coexist with the stable one. Bibliographic sources on the structure or lattice symmetries of these phases[56] are scarce, no confirmation exists if the data correspond to the stable phase. Therefore, although the stable melting phase diagram is very difficult to obtain in an experimental way, Oonk's equal-Gibbs energy method, along with the crossed isodimorphism concept,[57−59] provides a powerful tool of how to infer it from a thermodynamic point of view.

The stable crystalline phases Cr_{7OCB} and Cr_{9OCB} are probably nonisostructural forms. The concept of crossed isodimorphism assumes the existence of two-single loops [Cr_{7OCB}+N] and [SmA+Cr_{9OCB}] together with the partially second-order transition line, SmA_d-to-N, that has been calculated in Section 6.2, crossing every other. An important part of the analysis consists in finding the metastable ends of these loops: the metastable transition point $Cr_{7OCB} \rightarrow$ N in pure 9OCB and $Cr_{9OCB} \rightarrow SmA_d$ in pure 7OCB. Following the methodology referred to in a previous work,[21] some DSC experimental data (full squares in Figure 7) actually correspond to the liquidus (the upper equilibrium line) of the [Cr_{7OCB}+N] and [SmA+Cr_{9OCB}] loops in such a way that the required information can be extracted by extrapolating the known stable parts of the related loops. The chosen values for the metastable temperatures have been 200 and 208 K for pure 7OCB ($Cr_{9OCB} \rightarrow$ SmA) and 9OCB ($Cr_{7OCB} \rightarrow$ N), respectively. Due to the lack of information, the melting entropy of each metastable crystalline phase was taken to be the same as that of the corresponding stable crystalline phase. It should be noted that the results of the analysis remain largely unchanged by modifications of the above parameters if no

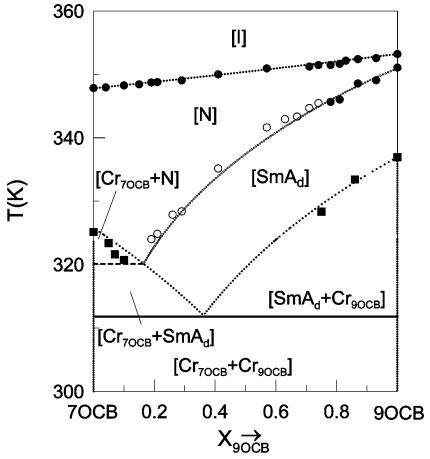

Figure 7. Tentative stable melting phase diagram for 7OCB+9OCB mixtures calculated through the Oonk's equal-Gibbs energy analysis. Full squares are DSC measurements.

miscibility exists in the solid-crystalline state. The results, expressed as Redlich−Kister polynomials, are

$$G^{E,\mathrm{Cr_{7O}}CB}(X) = X(1-X)[10000 + 100(1-2X)]\ \mathrm{J\ mol^{-1}} \quad (9a)$$

$$G^{E,\mathrm{Cr_{9OCB}}}(X) = X(1-X)[10000]\ \mathrm{J\ mol^{-1}} \quad (9b)$$

The calculated melting phase diagram, depicted in Figure 7, represents the possible attainable stable phase equilibrium. From a theoretical point of view, the crossing between the [Cr_{7OCB}+N] liquidus line and the second-order transition line SmA_d-to-N leads to a pseudo-invariant line at 320.1 K ($0 \le X_{9OCB} \le 0.17$), where the [Cr_{7OCB}+SmA] coexistence domain would change to the [Cr_{7OCB}+N] one. As for the eutectic three-phase equilibrium [Cr_{7OCB}+SmA+Cr_{9OCB}], the thermodynamic calculation leads to a temperature of 311.8 K. No experimental evidence on the pseudo- or on the eutectic invariant have been obtained in this work because, as for 7OCB+8OCB,[21] long aging is generally needed to reach the demixing between both solid-crystalline stable phases, Cr_{7OCB} and Cr_{9OCB}.

7.2. Tricritical Point Temperatures. This section addresses the issue if the tricritical behavior for the RN-to-SmA_d phase transition exists in a similar way as for the SmA_d-to-N phase transition. In such a hypothetical situation, if a tricritical point is found for the SmA_d-to-N phase transition, then it should also be found for the RN-to-SmA_d phase transition. Unfortunately, from an experimental point of view, the two-component systems showing re-entrant nematic behavior and also displaying tricritical points on the SmA_d-to-N transition are very scarce. If we also consider the possibility of a stable re-entrant nematic behavior that can be experimentally accessible by means of very precise measurements, the number of possible candidates drops even more. Another approach to answer the question could be driven by the thermodynamic assessment of tricritical points through the Oonk's equal-Gibbs energy analysis. The main idea of how a tricritical point could be inferred is drawn in Figure 8. In such a figure, there are several sets of Gibbs energy differences ($G^{SmA} - G^{I}$) and ($G^{N} - G^{I}$), one set for each chosen temperature. At 345 K, both Gibbs energy difference functions are crossing each other at the EGC in such a way that on the left composition side the N mesophase is more stable than the SmA_d one, changing this stability ranking at the right composition side from the EGC. Clearly, this change of stability takes place through a first-order transition because both ($G^{SmA} - G^{I}$) and ($G^{N} - G^{I}$) have different values around the EGC, implying

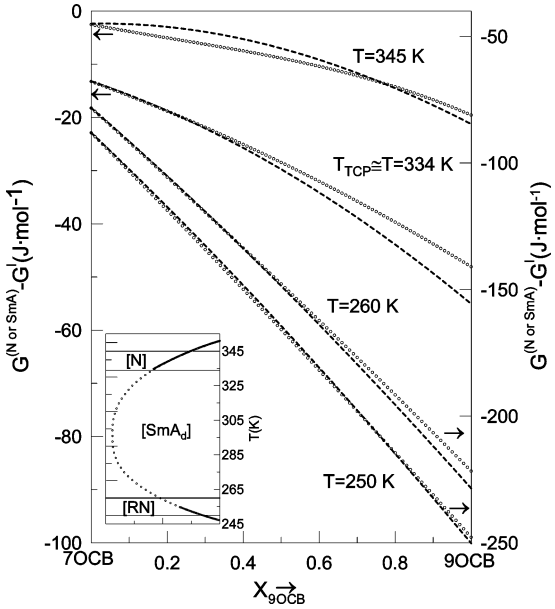

Figure 8. Calculated ($G^{N} - G^{I}$) (○○○○) and ($G^{SmA} - G^{I}$) (dashed lines) at several temperatures plotted against composition. The inset shows the calculated smectic−nematic phase boundary in the composition−temperature plane. First-order (continuous line) and second-order (dashed line) phase transitions are clearly distinguished. The horizontal lines on the inset correspond to temperatures for which Gibbs energy differences have been calculated. The two curves at the top are represented with respect to the left vertical axis. The two curves at the bottom are represented with respect to the right vertical axis.

that the original Gibbs energy functions G^{SmA} and G^{N} are different. The situation is similar to what is found at 250 K, although the differences between ($G^{SmA} - G^{I}$) and ($G^{N} - G^{I}$) are much more subtle. To sum up, first-order transitions exist between smectic and nematic mesophases at 345 and 250 K, but at low temperature, as can be observed on the inset, this would correspond to a RN-to-SmA_d phase transition. So, what happens between both temperatures? Let us consider the other two sets of Gibbs energy differences ($G^{SmA} - G^{I}$) and ($G^{N} - G^{I}$) for the other two represented temperatures in Figure 8. It is clearly shown that, on the right composition side (close to pure 9OCB), both G^{SmA} and G^{N} are different, the SmA_d being the more stable mesophase. When at constant temperature, we move toward the left composition side (increasing the content in 7OCB); both ($G^{SmA} - G^{I}$) and ($G^{N} - G^{I}$) come closer, but no crossing each other is observed. Only a coincidence between them (assuming a numerical discrepancy of about 0.01 J mol^{-1} or even more in both Gibbs energies) can be reported on counting from a certain composition toward the left composition side. That is to say, in this range, both G^{SmA} and G^{N} are indistinguishable in such a way that both mesophases virtually have the same Gibbs energy. As a criterion in such a calculation, when this situation takes place, a second-order transition occurs with the right EGC limit being the second-order transition point. WINIFIT software automatically performs these calculations for each temperature (every 0.05 K) over all temperatures for which the re-entrant behavior exists. The estimated tricritical point temperatures have been about 334 K on the SmA_d-to-N transition line and about 254 K on the RN-to-SmA_d transition one (see the inset of Figure 8). The first one is experimentally accessible, as can be observed in Figure 9. Figure 9A shows a linear relationship between $(\Delta H_{SmA-N})^{0.5}$ data and the temperature at which the experimental SmA_d-to-N transition occurs. Extrapolation to zero latent heat leads to a tricritical temperature of about 343 K, very close to that inferred from the thermo-

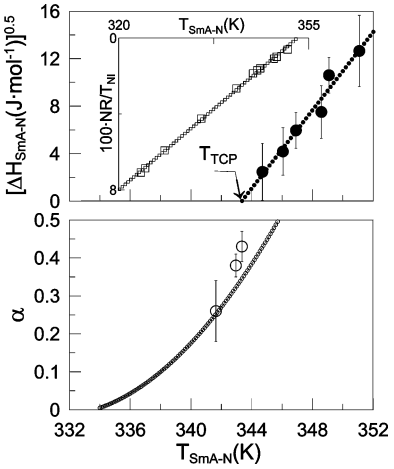

Figure 9. (A) Square-root latent heat ($[\Delta H_{SmA-N}]^{0.5}$) and (B) effective critical exponent α against T_{SmA-N} along with the representative curve calculated from eq 10 taking into account the linear relationship between NR/T_{NI} and T_{SmA-N}. On the inset, the transition temperature T_{SmA-N} is plotted against 100 times the normalized nematic range ($100NR/T_{NI}$).

dynamic assessment. Figure 9B shows an alternative approach based on the specific-heat critical exponent α to obtain information about the tricritical temperature. Unfortunately, no more than three α-exponents have been obtained from specific-heat measurements with a certain accuracy (see Table 2). Even so, the trend of these data seems to go to a similar tricritical temperature, as seen in Figure 9A.

Finally, it would be interesting to test the coherence of the α-exponents shown in Figure 9B. As proposed in a recent paper,[21] there seems to exist an empirical law representative of a common critical behavior displayed by the cyanobiphenyl compounds, either *n*CB or *n*OCB, which can be well-represented by the relationship

$$\alpha = 397(NR/T_{NI})^2 - 40.5(NR/T_{NI}) + 1.02 \qquad (10)$$

in terms of α-values and NR/T_{NI} (the nematic range normalized by the N-to-I transition temperature T_{NI}). On the inset, in Figure 9A, a linear trend exists between the NR/T_{NI} and the T_{SmA-N} for the 7OCB+9OCB mixtures in a broad temperature range in such a way that eq 10 can be easily translated in terms of α-values and T_{SmA-N}. The representative curve has been drawn in Figure 9B along with the experimental α-values. Regardless of whether the accord between the α-values and the representative curve is good enough, the critical behavior in the SmA_d-to-N transition not only seems to be coherent in relation to other cyanobiphenyl compounds but is also intrinsically consistent with the thermodynamic Oonk's EGC approach.

8. Concluding Remarks

The two-component system 7OCB+9OCB provides an excellent example of monotropic re-entrant nematic behavior. The experimental phase diagram was established with the aid of MDSC and optical microscopy. In addition, a complete thermodynamic analysis was performed in order to represent quite well the monotropic re-entrant behavior in a temperature−composition plane as well as to get two tricritical points, one of them on the SmA_d-to-N phase transition and another on the RN-to-SmA_d phase transition. This fact proves that the critical behavior seems to be comparable irrespective of if the phase transition to a SmA_d mesophase from N or RN mesophases occurs.

Experimental evidence for the SmA_d-to-N tricritical point were obtained from latent heat determinations as well as from specific-heat critical exponents. However, the existence of the RN-to-SmA_d tricritical point was not experimentally attained. The thermodynamic analysis enables us to obtain the possible melting phase diagram.

Acknowledgment. The authors are grateful for financial support from the MCYT of Spain (project FIS2005-00975) and from the Generalitat de Catalunya (DURSI grant 2005SGR-00535). D.O.L. acknowledges Gobierno Vasco for an invited position at the University of the País Vasco.

References and Notes

(1) Cladis, P. E. *Phys. Rev. Lett.* **1975**, *35*(1), 48.
(2) Pelzl, G.; Diele, S.; Latif, I.; Weissflog, W.; Demus, D. *Cryst. Res. Technol.* **1982**, *17*, K78.
(3) Diele, S.; Pelzl, G.; Latif, I.; Demus, D. *Mol. Cryst. Liq. Cryst.* **1983**, *92*, 27.
(4) Cladis, P. E.; Bogardus, R. K.; Daniels, W. B.; Taylor, G. N. *Phys. Rev. Lett.* **1977**, *39*(11), 720.
(5) Cladis, P. E.; Bogardus, R. K.; Aasden, D. *Phys. Rev. A* **1978**, *18*(5), 2292.
(6) Pershan, P. S.; Prost, J. *J. Phys. Lett.* **1979**, *40*, L-17.
(7) Cladis, P. E.; Guillon, D.; Bouchet, F. R.; Finn, P. L. *Phys. Rev. A* **1981**, *23*(5), 2594.
(8) Longa, L.; de Jeu, W. H. *Phys. Rev. A* **1982**, *26*, 1632.
(9) Berker, A. N.; Walker, J. S. *Phys. Rev. Lett.* **1981**, *47*(20), 1469.
(10) Indekeu, J. O.; Berker, A. N. *Phys. Rev. A* **1986**, *33*, 1158.
(11) Indekeu, J. O.; Berker, A. N.; Chiang, C.; Garland, C. W. *Phys. Rev. A* **1987**, *35*(3), 1371.
(12) Netz, R. R.; Berker, A. N. *Phys. Rev. Lett.* **1992**, *68*, 333.
(13) Sear, R. P.; Jackson, G. *Mol. Phys.* **1994**, *83*, 961.
(14) Sear, R. P.; Jackson, G. *Phys. Rev. Lett.* **1995**, *74*, 4261.
(15) de Miguel, E.; Martín del Río, E. *Phys. Rev. Lett.* **2005**, *95*, 217802.
(16) Klug, D. D., Whalley E. *J. Chem. Phys.* **1979**, *71*, 1874.
(17) Clark, N. A. *J. Phys., Colloq.* **1979**, *40*, C3−345.
(18) Oonk, H. A. J. *Phase Theory. The Thermodynamics of Heterogeneous Equilibria*; Elsevier: Amsterdam, 1981.
(19) Van Hecke, G. R. *J. Phys. Chem.* **1985**, *89*, 2058.
(20) Sorenson, J. M.; Van Hecke, G. R. *J. Phys. Chem.* **1994**, *98*, 10289.
(21) Sied, M. B.; Salud, J.; López, D. O.; Allouchi, H.; Diez, S.; Tamarit, J. Ll. *J. Phys. Chem. B* **2003**, *107*, 7820.
(22) Lushington, K. J.; Kasting, G. B.; Garland, C. W. *Phys. Rev. B* **1980**, *22*(5), 2569.
(23) Ema, K.; Nounesis, G.; Garland, C. W.; Shashidhar, R. *Phys. Rev. A* **1989**, *39*, 2599.
(24) Guillon, D.; Cladis, P. E.; Stamatoff, J. *Phys. Rev. Lett.* **1978**, *41*(23), 1598.
(25) Kortan, A. R.; von Känel, H.; Birgenau, R. J.; Litster, J. D. *Phys. Rev. Lett.* **1981**, *47*, 1206.
(26) Kortan, A. R.; von Känel, H.; Birgenau, R. J.; Litster, J. D. *J. Phys. (Paris)* **1984**, *45*, 529.
(27) Chen, N. R.; Hark, S. K.; Ho, J. T. *Phys. Rev. A* **1981**, *24*(5), 2843.
(28) Brodzik, M.; Dabrowski, R. *Liq. Cryst.* **1995**, *18*(1), 61.
(29) Brodzik, M.; Dabrowski, R. *Liq. Cryst.* **1996**, *20*(1), 99.
(30) Prasad, S. K.; Nair, G. G. *Adv. Mater.* **2001**, *13*, 40.
(31) Dong, R. Y. *J. Chem. Phys.* **1981**, *75*, 2621.
(32) Shen, X.; Dong, R. Y. *J. Chem. Phys.* **1998**, *108*, 9177.
(33) Bharatam, J.; Bowers, C. R. *J. Phys. Chem. B* **1999**, *103*, 2510.
(34) Dong, R. Y.; Cheng, M. *J. Chem. Phys.* **2000**, *113*, 3466.
(35) Nozaki, R.; Bose, T. K.; Yagihara, S. *Phys. Rev. A* **1992**, *46*, 7733.
(36) Urban, S.; Dabrowski, R.; Gestblom, B.; Kocot, A. *Liq. Cryst.* **2000**, *27*(12), 1675.
(37) Gupta, M.; Dhal, R.; Agrawal, V. K.; Dabrowski, R.; Tykarsaka, M. *Phys. Rev. E* **2005**, *72*, 021703.
(38) Bhattacharya, S.; Letcher, S. V. *Phys. Rev. Lett.* **1980**, *44*, 414.
(39) Jadzyn, J.; Czechowski, G. *Phys. Rev. E* **2001**, *64*, 052702.
(40) Johnson, C. S.; Collings, P. J. *J. Chem. Phys.* **1983**, *79*, 4056.
(41) Żywociński, A. *J. Phys. Chem. B* **1999**, *103*, 3087.
(42) Sied, M. B.; Salud, J.; López, D. O.; Barrio, M.; Tamarit, J. Ll. *Phys. Chem. Chem. Phys.* **2002**, *4*, 2587.
(43) McMillan, W. L. *Phys. Rev. A* **1971**, *4*, 1238.
(44) Kobayashi, K. *Phys. Lett.* **1970**, *31A*, 125.
(45) De Gennes, P. G.; Prost, J. *The Physics of Liquid Crystals*; Oxford Science Publications: Oxford, U.K., 1994.
(46) Diez, S.; López, D. O.; De la Fuente, M. R.; Pérez-Jubindo, M. A.; Salud, J.; Tamarit, J. Ll. *J. Phys. Chem. B* **2005**, *109*, 23209.

(47) Diez, S.; Pérez-Jubindo, M. A.; De la Fuente, M. R.; López, D. O.; Salud, J.; Tamarit, J. Ll. *Chem. Phys. Lett.* **2006**, *423*, 463.

(48) Wunderlich, B.; Boller, A.; Okazaki, I.; Kreitmeier, S. *Thermochim. Acta* **1996**, *282/283*, 143.

(49) Hatta, I.; Ichikawa, H.; Todoki, M. *Thermochim. Acta* **1995**, *267*, 83.

(50) Thoen, J.; Marynissen, H.; van Dael, W. *Phys. Rev. Lett.* **1984**, *52*(3), 204.

(51) Lafouresse, M. G.; Sied, M. B.; Allouchi, H.; López, D. O.; Salud, J.; Tamarit, J. Ll. *Chem. Phys. Lett.* **2003**, *376*, 188.

(52) Sied, M. B.; Diez, S.; Salud, J.; López, D. O.; Cusmin, P.; Tamarit, J. Ll.; Barrio, M. *J. Phys. Chem. B* **2005**, *109*, 16284.

(53) Kumar, S. *LIQUID CRYSTALS*: *Experimental Study of Physical Properties and Phase Transitions*; Cambridge University Press: Cambridge, U.K., 2001.

(54) Daranas, D.; López, R.; López, D. O. *WINIFIT 2.0 Computer Program*, Polythecnical University of Catalonia, Barcelona, Spain, 2000.

(55) Cusmin, P.; de la Fuente, M. R.; Salud, J.; Pérez-Jubindo, M. A.; López, D. O.; Diez, S.; Barrio, M.; Tamarit, J. Ll. *Int. Liq. Cryst. Conf.* **2006**, *Abstract 3197*.

(56) Das, M. K.; Paul, S.; Paul, R. *Mol. Cryst. Liq. Cryst. Sci. Technol. Sect. A* **1995**, *264*, 89.

(57) Sied, M. B.; López D. O.; Tamarit, J. Ll.; Barrio, M. *Liq. Cryst.* **2002**, *29*(1), 57.

(58) Salud, J.; López, D. O.; Tamarit, J. Ll.; Barrio, M.; Jacobs, M. H. G.; Oonk, H. A. J. *J. Solid State Chem.* **2000**, *154*, 390.

(59) Pardo, L. C.; Barrio, M.; Tamarit, J. Ll.; Negrier, P.; López, D. O.; Salud, J.; Mondieig, D. *J. Phys. Chem.. B* **2001**, *105*(42), 10326.